Mixing by shear instability at high Reynolds number

W. R. Geyer,[1] A. C. Lavery,[1] M. E. Scully,[2] and J. H. Trowbridge[1]

Received 27 August 2010; revised 4 October 2010; accepted 8 October 2010; published 25 November 2010.

[1] Shear instability is the dominant mechanism for converting fluid motion to mixing in the stratified ocean and atmosphere. The transition to turbulence has been well characterized in laboratory settings and numerical simulations at moderate Reynolds number—it involves "rolling up", i.e., overturning of the density structure within the cores of the instabilities. In contrast, measurements in an energetic estuarine shear zone reveal that the mixing induced by shear instability at high Reynolds number does not primarily occur by overturning in the cores; rather it results from secondary shear instabilities within the zones of intensified shear separating the cores. This regime is not likely to be observed in the relatively low Reynolds number flows of the laboratory or in direct numerical simulations, but it is likely a common occurrence in the ocean and atmosphere. **Citation:** Geyer, W. R., A. C. Lavery, M. E. Scully, and J. H. Trowbridge (2010), Mixing by shear instability at high Reynolds number, *Geophys. Res. Lett.*, *37*, L22607, doi:10.1029/2010GL045272.

1. Introduction

[2] The structure and dynamics of shear instability have mainly been investigated at low Reynolds number (Re = $u\delta/\nu$, where u is one half the velocity difference across the layer, δ is the half-width of the shear zone, and ν is the kinematic viscosity of the fluid) in laboratory facilities [*Thorpe*, 1973; *Caulfield et al.*, 1996; *Koop and Browand*, 1979] and numerical simulations [*Smyth et al.*, 2001], with only limited observations in field settings at high Re [*Smyth et al.*, 2001; *Hebert et al.*, 1992]. Laboratory studies of shear instability [*Thorpe*, 1973; *Caulfield et al.*, 1996; *Koop and Browand*, 1979] as well as direct numerical simulations [*Caulfield and Peltier*, 2000; *Smyth et al.*, 2001] show that turbulent mixing occurs primarily in the cores of shear instabilities, due to gravitational collapse of the statically unstable fluid rolled up within the cores (Figure 1a). Moreover, *Corcos and Sherman* [1976] hypothesize that secondary instability should lead to mixing *within the braids* (i.e., the thin filaments connecting the cores at high Reynolds number (Figure 1b)). They suggest that most atmospheric instabilities would have high enough Re to have mixing within the braids, and that more energetic oceanic mixing would exhibit similar behavior. Two-dimensional numerical experiments by *Staquet* [1995] and *Smyth* [2003] show that secondary instabilities do occur in the braids for sufficiently high Re, although the 2-d simulations could not simulate the onset of turbulence. *Atsavapranee and Gharib* [1997] demonstrate in a laboratory study that secondary instabilities occur along the braids of primary instabilities at Re ~ 2,000.

[3] Whereas shear instabilities at high Re have commonly been observed in the ocean using acoustic backscatter and turbulence-resolving sensors [*Seim and Gregg*, 1994; *Geyer and Smith*, 1987; *Moum et al.*, 2003; *Tedford et al.*, 2009; *Farmer and Armi*, 1989], none of these turbulence measurements resolve the spatial structure of the braids and cores adequately to test the conjecture by Corcos and Sherman of braid-induced mixing. Here we present observations of shear instabilities occurring in a highly stratified estuary, measured using a combination of acoustic imaging and in situ measurements of the turbulent velocity and density distributions. These observations provide new information about the distribution of turbulent mixing within the instabilities, supporting the conjecture of *Corcos and Sherman* [1976] that secondary instabilities of spanwise vorticity within the braids play an essential role in mixing at high Re.

2. Methods

[4] Measurements were conducted at two along-river transects in the Connecticut River estuary in November 2008 and again in November 2009. River discharge was moderate (600–800 m^3/s) during both the 2008 and 2009 deployments, yielding high stratification conditions. Acoustic backscatter profiles were obtained with a 4-channel broadband Edgetech echo sounder [*Lavery et al.*, 2010]. In situ measurements of velocity, conductivity and temperature were obtained at 8 vertical locations on a 10-m, rigid instrument package that is suspended from a research vessel (as described by *Geyer et al.* [2008]). Each instrument bracket contains three co-located sensors: 1) a Sontek acoustic Doppler velocimeter (25Hz sampling rate); 2) a Seabird Electronics SBE-7 microconductivity probe (300Hz sampling rate); and 3) an RBR conductivity, pressure and depth (CTD) sensor (6 Hz sampling rate). During most of the measurements, the echo sounder was mounted on the opposite side of the vessel from the instrument frame, causing significant phase shift and some decorrelation between the acoustic and in situ measurements. However, similar wave structures were observed at both sensor locations. The observations presented here were conducted during the ebb tide near the mouth of the estuary, with the vessel repeatedly sampling the water column downstream of major constrictions in the estuary. Most of the sampling was performed while steaming slowly upstream against the ebbing current, and during one ebb tide measurements were made at an anchor station approximately 300 m downstream of a constriction.

3. Results

[5] Acoustic images reveal trains of shear instability waves in the pycnocline within the Connecticut River estuary

[1]Woods Hole Oceanographic Institute, Woods Hole, Massachusetts, USA.
[2]Center for Coastal Physical Oceanography, Old Dominion University, Norfolk, Virginia, USA.

0094-8276/10/2010GL045272

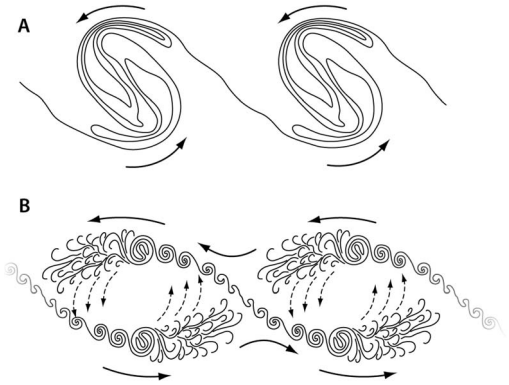

Figure 1. Schematic of mixing by Kelvin-Helmholtz instability (a) at low Reynolds number (based on numerical simulation at Re = 1,000 by *Smyth et al.* [2001] (4), and (b) at high Reynolds number (based on the observations in this study at Re = 500,000).

(Figure 2a) and just seaward of the mouth (Figure 2b) during the ebb tide. The acoustic scattering is most intense in regions of strong density gradient, as noted by *Moum et al.* [2003] and confirmed by the in situ measurements in this study. The surface velocity was strongly seaward, and the bottom current was weak. In both cases the flow passed through a minimum in cross-sectional area (defined as x = 0), and the maximum amplitude shear instability waves occurred 150–300 m downstream of the constriction. The spatial distribution and structure of the instabilities varied from transect to transect, but frequent shear instabilities were consistently observed around the time of maximum surface outflow, with peak-to-trough heights of 1–3 m. The upper image indicates a group of unstable waves that appears to be growing spatially, but the lower image indicates multiple waves of comparable amplitude and roughly constant form, suggesting that the spatial growth has been arrested, even though in both cases the large-scale tilt of the interface indicates that the overall shear is being baroclinically forced.

[6] Detailed views of instabilities from the two sampling locations (Figure 3) reveal the familiar braid and core structure of Kelvin-Helmholtz instabilities [*Thorpe*, 1973; *Koop and Browand*, 1979]. Accompanying velocity and salinity profiles show strong salinity gradients and shears through the pycnocline. Note that the vertical spacing of the sensors is too coarse to resolve the details of the structure that is evident in the echo sounding traces; however, the high horizontal resolution provides more insight into the structure, as will be discussed below. The gradient Richardson number ($Ri = N^2/(\partial u/\partial z)^2$ where $N^2 = -(g/\rho)\partial\rho/\partial z$ is the square of the buoyancy frequency and $\partial u/\partial z$ is the vertical shear) was calculated based on 5-second averages of the density and velocity gradients, providing a rough indication of shear instability. Ri showed a local minimum at the center of the shear instabilities (shown as a dashed line on Figure 3), with values typically falling between 0.2 and 0.25. The sensor spacing was too coarse to determine the minimum value of Ri within the pycnocline, but these estimates indicate that conditions were favorable for the formation of instabilities based on linear theory [*Hazel*, 1972; *Drazin and Reid*, 1981].

[7] The wavelengths of the waves were estimated based on their apparent periods and propagation speed relative to the vessel, which was determined by the relative velocity at the center of the instabilities, where the wave velocity is equal to the celerity [*Miles*, 1961]. The large instabilities have estimated wavelengths of approximately 10-m. This wavelength is consistent with instabilities originating from a shear-layer thickness of 1.5–2 m, based on linear theory [*Hazel*, 1972]. This is roughly consistent with the shear-layer thickness at the location of the instabilities, suggesting that the initial thickness of the shear layer was not much smaller than its value at the time of these observations. The braids also exhibit what appear to be secondary instabilities in the same plane as the primary instability (i.e., the roll-up of spanwise vorticity), with a range of wavelengths from 0.5 to 2 m.

[8] The relationship between the acoustic imagery and the turbulence was best resolved during stationary measurements at the location of the largest instabilities, about 300-m downstream of the inner constriction. A large set of unstable waves was observed during mid-ebb (Figure 4), at the same location and same phase of the tidal cycle as the observations in Figure 2a. The instabilities are 13–17-m long (based on an estimated propagation speed of 0.4 m/s), longer but otherwise similar to the underway observations. The in situ instruments provide crude vertical resolution of the density structure corresponding to the instabilities (Figure 4, middle), but its temporal variability was very finely resolved (Figure 4, bottom). The braid-core structure could still be discerned by the density measurements, although the vertical gradients within the braids were underestimated. The acoustic sensor was displaced laterally by 6 m, so the density structure could not be mapped directly onto the acoustic image. However many of the same features were observed in the in situ observations as the acoustics, with some distortion due to the shear. As found in other studies [*Seim and Gregg*, 1994; *Tedford et al.*, 2009] , the regions of strong vertical density gradient exhibit

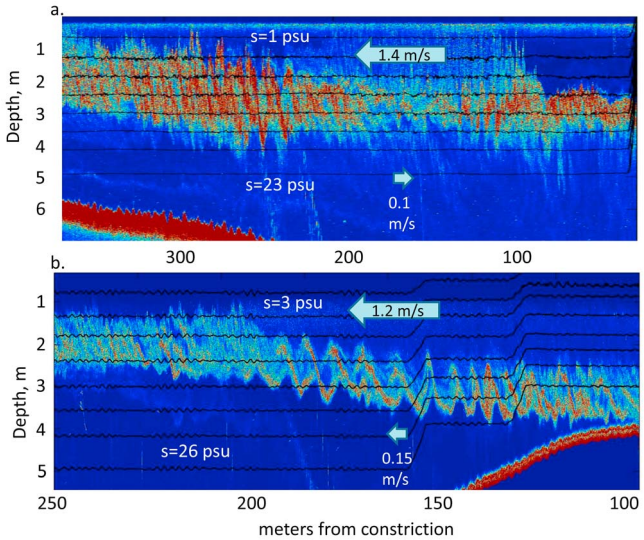

Figure 2. Echo sounding images of (a) inner transect and (b) outer transect. The high acoustic backscattering in associated with regions of large density gradients within the pycnocline. Shear instabilities are evident in both images, with amplitudes of 1–3 m. The seabed is visible in part of each image. Spatially averaged near-surface and near-bottom velocity and salinities are indicated. The depth of the shipboard sensors is indicated by black lines.

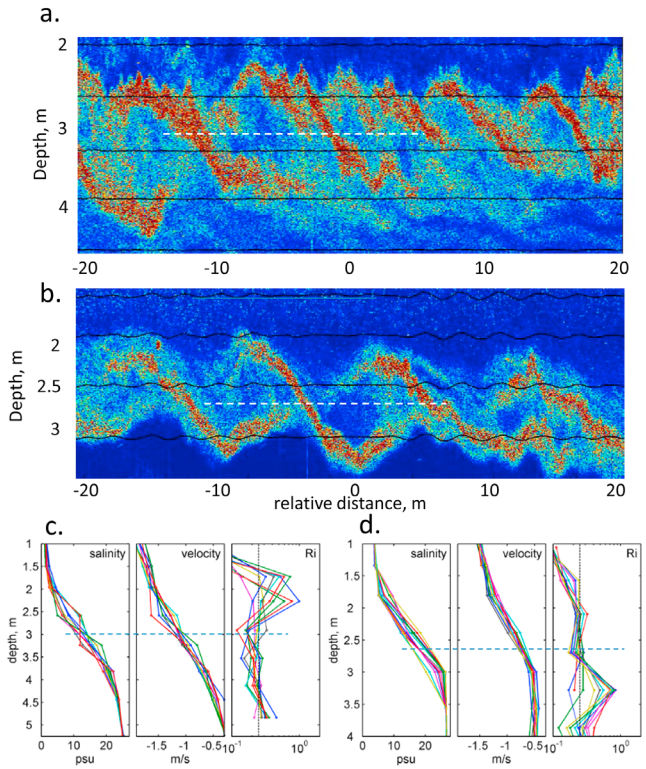

Figure 3. Detail of shear instabilities in (a) inner transect and (b) outer transect. (c and d) Salinity, relative velocity and Ri profiles at roughly 5-m intervals are shown for two images. Ri profiles are based on 5-s (roughly 5-m) averages of shear and stratification. Dashed lines indicate the center of the instabilities (based on the inflection point of the braid).

high backscatter, whereas the homogeneous regions have relatively weak acoustic returns.

[9] The spatial structure of the turbulence was best resolved by the high-frequency conductivity sensors. The variance of high-pass filtered conductivity (frequencies 10–100 Hz) is indicated by color-coded dots and superimposed on the density structure in Figure 4 (middle). The variance in this band is within the inertial-convective and viscous-convective subranges of the salinity spectrum; thus it provides a qualitative indication of where turbulent mixing of salt is occurring. The high conductivity variance is almost exclusively localized to the braids of the instabilities, with much lower values of conductivity variance within the cores. The spatial distribution of conductivity variance is consistent with the acoustic backscatter distribution, which shows quiet conditions within the cores (indicated by "C" in Figure 4) and intense backscatter in the braids (indicated by "B"). Although the local gradients were highest in the center of the braid, the high-frequency variations of salinity indicate that most of the mixing occurred in the downstream extension of the braid (marked as "M"). These mixing zones appeared to be more extensive in the upper limb of the braid; however this is due to the greater relative motion in the upper water column. The turbulence analysis presented below indicates that the turbulence levels were comparable.

[10] The magnitude of the dissipation of scalar variance of salinity χ_s and dissipation of turbulent kinetic energy ε were estimated for 10–15 second intervals (shown in Figure 4, middle) within the instability, in order to characterize the intensity of turbulence within the cores and the braids. Following *Shaw and Trowbridge* [2001], ε was estimated from the inertial subrange of vertical velocity variance, and χ_s was estimated based on the inertial subrange and viscous-convective subrange of salinity variance (note that virtually all of the conductivity variance is due to salinity in this environment). The result of this analysis (Table 1) show that χ_s is considerably elevated in the braid mixing zones relative to the cores. The center of the braid (Interval 2) shows a more modest elevation in dissipation rates, but that segment extends into the cores on either side, reducing the average rates for that interval (note that shorter data segments would not yield statistically significant estimates). Estimates of ε do not show the marked reduction in the cores that are seen in χ_s—apparently turbulence continues within the weakly stratified cores after the salinity has been homogenized, but the χ_s distributions clearly indicate that the mixing of salt occurs almost exclusively in the braids.

[11] Estimates of the Ozmidov scale $L_o = (\varepsilon/N^3)^{1/2}$ (where N is the local buoyancy frequency) are also shown in Table 1, providing an indication of the scales of the turbulent eddies. The Ozmidov scale is only 5 cm within the braid, and it ranges from 10 to 30 cm in the braid mixing zone—much smaller than the overall scale of the primary instabilities, consistent

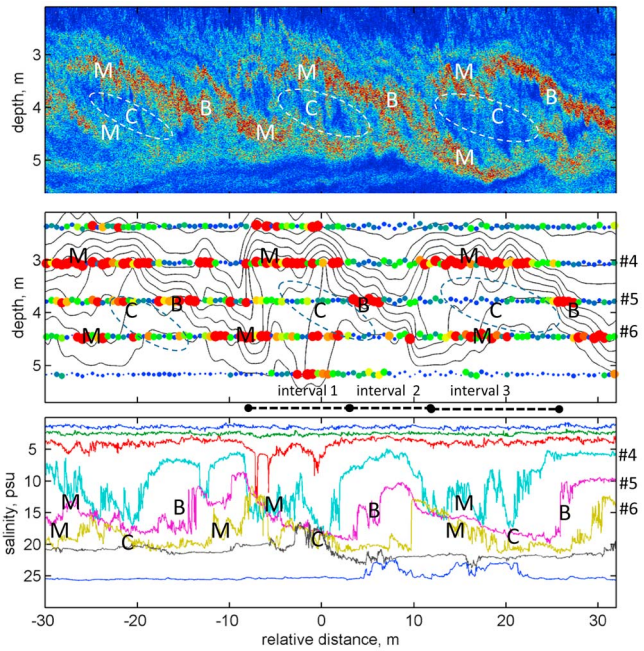

Figure 4. (top) Comparison of acoustic imagery to in situ measurements of the salinity structure, shown as (middle) contours and as (bottom) timeseries plots, within instabilities observed at the anchor station. The intensity of high-passed (10–200 Hz) salinity variance is indicated by colored dots superimposed on the salinity contours in Figure 4 (middle) (red > 0.1 psu2, blue < 0.01psu2). In all of the plots, the "B" symbols indicate the approximate center of the braid; "C" indicates the core, and "M" indicates the mixing zone "downstream" of the braid in a coordinate system moving with the instability. The three intervals for calculation of turbulence quantities are shown between Figures 4 (middle) and 4 (bottom).

Table 1. Dissipation Rates of Salinity Variance χ_s, Turbulent Kinetic Energy ε, Buoyancy Frequency N and Ozmidov Scale L_o in Different Parts of the Shear Instabilities

Sensor	Location	χ_s ($psu^2 s^{-1}$)	ε ($m^2 s^{-3}$)	N(s^{-1})	L_o(m)
		Interval 1			
#4	braid mixing zone	**0.24**	**3.1×10^{-4}**	0.35	0.08
#5	core	0.04	3.0×10^{-4}	0.05	1.50
#6	braid mixing zone	**0.45**	**6.8×10^{-4}**	0.20	0.29
		Interval 2			
#4	above	0.03	0.1×10^{-4}	0.10	0.10
#5	braid	0.10	0.8×10^{-4}	0.30	0.05
#6	below	0.07	1.5×10^{-4}	0.10	0.39
		Interval 3			
#4	braid mixing zone	**0.32**	**2.1×10^{-4}**	0.35	0.07
#5	core	0.01	1.0×10^{-4}	0.10	0.32
#6	braid mixing zone	**0.27**	**3.0×10^{-4}**	0.20	0.19

with the hypothesis of localized mixing within the braids. Only within the cores is the stratification weak enough that the Ozmidov scale approaches that scale. The most intense mixing occurs "downstream" of the inflection point of the braid, considering a reference frame that moves with the instability. Mixing develops on both the upward and lower limb of the braid, and becomes most intense about ½ wavelength downstream. The mixing appears to be initiated by secondary instabilities, which are evident as fluctuations with roughly 1-m wavelength on the braids (evident both in the echo-sounder data and the timeseries of salinity). The wavelengths of the observed secondary instabilities are consistent with a braid thickness of around 20 cm. Given the overall velocity difference of about 1 m/s, the local shear rate within the braid should have been 5 s^{-1}. This amplification of shear is consistent with *Smyth*'s [2003] 2-dimensional simulations of high Re instabilities. Defining Ri_o as the overall value of Ri and Ri_b as its minimum value in the braid, $Ri_b/Ri_o = \delta_b/\delta_o$, so $Ri_b \sim 0.05$, yielding near maximal growth rates (within ~20%) for the secondary instabilities. An approximate advective timescale between the center of the braid and the end of the mixing zone is $T_a = \lambda_b/2(\Delta u/4)$ (where $\lambda_b/2$ is half the wavelength of the primary instability, and $\Delta u/4$ is the approximate advective speed of the fluid on either side of the braid relative to the stagnation point). For these observations, this advective timescale is 15–20 seconds, or 75 to 100 shear timescales (based on the shear within the braid). This is approximately the non-dimensional timescale required for the full development and collapse of shear instabilities [*Thorpe*, 1973; *Smyth et al.*, 2001] —thus there is adequate time within the dimensions of the primary instabilities for secondary instabilities to grow, collapse and mix. This "life-cycle" of secondary instability occurs on either side of the core, and the core is continually supplied mixed water by the secondary instabilities.

4. Discussion

[12] The most likely explanation for the difference in the structure of the instabilities in this study relative to prior laboratory studies and numerical simulations is the influence of Reynolds number. Re = 500,000 for these observations—several orders of magnitude higher than the highest values observed in the laboratory [*Thorpe*, 1973; *Koop and Browand*, 1979] or simulated in three-dimensional DNS calculations [*Caulfield and Peltier*, 2000; *Smyth et al.*, 2001]. Although turbulence does occur as low as Re = 1000 [*Thorpe*, 1973], at these low values the braids remain laminar until engulfed by the turbulence originating in the cores. In order for the braids to become turbulent, the Reynolds number at the scale of the braids needs to be adequately large. For stratified turbulent flows, the "buoyancy Reynolds number" $Re_b = \varepsilon/\nu N^2$ must exceed 20–30 in order for turbulence to be maintained [*Stillinger et al.*, 1983]. Based on an estimated braid thickness of 20 cm, Re_b = 100 –500 for these observations, far above the turbulence threshold. If we assume dynamic similarity, the turbulence threshold within the braids should occur when overall Reynolds number is around 50,000 (i.e., an order of magnitude less than its value in these observations). This is still a factor of 5 to 10 greater than the most energetic laboratory experiments and numerical simulations, but well within the range of Re expected in the ocean and atmosphere.

[13] The secondary instabilities responsible for the mixing at high Re occur much faster than the three-dimensional instabilities that occur at low Re, based on roughly a five-fold amplification of shear rate in the braid. The fully developed billows closely resemble the 2-dimensional simulations of *Staquet* [1995], but they differ in their subsequent evolution in that they do not exhibit collapse, but rather appear to stop evolving after the secondary instabilities develop. The secondary instabilities may provide a significant energy sink that arrests the growth of the primary instabilities, as originally hypothesized by *Corcos and Sherman* [1976]. The long trains of waves of large but nearly constant amplitude (Figure 2b), with no indication of either growth, pairing or collapse, may be the result of the "viscous" influence of the secondary instabilities.

[14] These observations suggest that, in analogy to unstratified, high Re flows, the kinematics appear to be self-similar at a range of scales set by the size of Re. The secondary instabilities rolling up within the braids appear to be of similar structure to the primary instabilities, and if Re is high enough, they should contain tertiary instabilities of similar form. Only at the scale that the braids become laminar should the structure of the instabilities revert to the familiar form observed in prior low-Re studies and sketched in Figure 1a. This smallest scale, embedded within the braids of the primary and secondary instabilities, is where mixing actually occurs. Based on this hypothesized self-similarity, the efficiency of mixing would not be expected to vary with Re.

[15] **Acknowledgments.** This research was supported by NSF grant OCE-0824871 and ONR grant N00014-0810495.

References

Caulfield, C. P., and W. R. Peltier (2000), The anatomy of the mixing transition in homogeneous and stratified free shear layers, *J. Fluid Mech.*, *413*, 1–47, doi:10.1017/S0022112000008284.

Caulfield, C. P., S. Yoshida, and W. R. Peltier (1996), Secondary instability and three-dimensionalization in a laboratory accelerating shear layer with varying density differences, *Dyn. Atmos. Oceans*, *23*, 125–138, doi:10.1016/0377-0265(95)00418-1.

Corcos, G. M., and F. S. Sherman (1976), Vorticity concentration and the dynamics of unstable free shear layers, *J. Fluid Mech.*, *73*, 241–264, doi:10.1017/S0022112076001365.

Drazin and Reid (1981), *Hydrodynamic Stability*, 525 pp., Cambridge Univ. Press, Cambridge, U. K.

Farmer, D. M., and L. Armi (1989), Stratified flow over topography: The role of small-scale entrainment and mixing in flow establishment, *Proc. R. Soc.*, *455*, 3221–3258.

Geyer, W. R., and J. D. Smith (1987), Shear instability in a highly stratified estuary, *J. Phys. Oceanogr.*, *17*, 1668–1679, doi:10.1175/1520-0485(1987)017<1668:SIIAHS>2.0.CO;2.

Geyer, W. R., M. E. Scully, and D. K. Ralston (2008), Quantifying vertical mixing in estuaries, *Environ. Fluid Mech.*, *8*, 495–509, doi:10.1007/s10652-008-9107-2.

Hazel, P. (1972), Numerical studies of the stability of inviscid stratified shear flows, *J. Fluid Mech.*, *51*, 39–61, doi:10.1017/S0022112072001065.

Hebert, D., J. N. Moum, C. A. Paulson, and D. R. Caldwell (1992), Turbulence and internal waves at the Equator. Part II: Details of a single event, *J. Phys. Oceanogr.*, *22*, 1346–1356, doi:10.1175/1520-0485(1992)022<1346:TAIWAT>2.0.CO;2.

Koop, C. G., and F. K. Browand (1979), Instability and turbulence in a stratified fluid with shear, *J. Fluid Mech.*, *93*, 135–159, doi:10.1017/S0022112079001828.

Lavery, A. C., D. Chu, and J. N. Moum (2010), Measurements of acoustic scattering from zooplankton and oceanic microstructure using a broadband echosounder, *ICES J. Mar. Sci.*, *67*, 379–394, doi:10.1093/icesjms/fsp242.

Miles, J. W. (1961), On the stability of heterogeneous shear flows, *J. Fluid Mech.*, *10*, 496–508, doi:10.1017/S0022112061000305.

Moum, J. N., D. M. Farmer, W. D. Smith, L. Armi, and S. Vagle (2003), Structure and generation of turbulence at interfaces strained by internal solitary waves propagating shoreward over the continental shelf, *J. Phys. Oceanogr.*, *33*, 2093–2112, doi:10.1175/1520-0485(2003)033<2093:SAGOTA>2.0.CO;2.

Seim, H. E., and M. C. Gregg (1994), Detailed observations of a naturally occurring shear instability, *J. Geophys. Res.*, *99*, 10,049–10,073, doi:10.1029/94JC00168.

Shaw, W. J., and J. H. Trowbridge (2001), the direct estimation of near-bottom turbulent fluxes in the presence of energetic wave motions, *J. Atmos. Oceanic Technol.*, *18*, 1540–1556, doi:10.1175/1520-0426(2001)018<1540:TDEONB>2.0.CO;2.

Smyth, W. D. (2003), Secondary Kelvin-Helmholtz instability in weakly stratified shear flow, *J. Fluid Mech.*, *497*, 67–98, doi:10.1017/S0022112003006591.

Smyth, W. D., J. N. Moum, and D. R. Caldwell (2001), The efficiency of mixing in turbulent patches: Inferences from direct simulations and microstructure observations, *J. Phys. Oceanogr.*, *31*, 1969–1992, doi:10.1175/1520-0485(2001)031<1969:TEOMIT>2.0.CO;2.

Staquet, C. (1995), Two-dimensional secondary instabilities in a stratified shear layer, *J. Fluid Mech.*, *296*, 73–126, doi:10.1017/S0022112095002072.

Stillinger, D. C., K. N. Helland, and C. W. Van Atta (1983), Experiments on the transition of homogeneous turbulence to internal waves in a stratified fluid, *J. Fluid Mech.*, *131*, 91–122, doi:10.1017/S0022112083001251.

Tedford, E. W., J. R. Carpenter, R. Pawlowicz, R. Pieters, and G. A. Lawrence (2009), Observation and analysis of shear instability in the Fraser River estuary, *J. Geophys. Res.*, *114*, C11006, doi:10.1029/2009JC005313.

Thorpe, S. A. (1973), Experiments on instability and turbulence in a stratified shear flow, *J. Fluid Mech.*, *61*, 731–751, doi:10.1017/S0022112073000911.

W. R. Geyer, A. C. Lavery, and J. H. Trowbridge, Woods Hole Oceanographic Institute, Mail Stop 12, Woods Hole, MA 02543, USA. (rgeyer@whoi.edu)

M. E. Scully, Center for Coastal Physical Oceanography, Old Dominion University, 4111 Monarch Way, 3rd Floor, Norfolk, VA 23508, USA.